Lab on a Chip

Accepted Manuscript

This is an *Accepted Manuscript*, which has been through the Royal Society of Chemistry peer review process and has been accepted for publication.

Accepted Manuscripts are published online shortly after acceptance, before technical editing, formatting and proof reading. Using this free service, authors can make their results available to the community, in citable form, before we publish the edited article. We will replace this *Accepted Manuscript* with the edited and formatted *Advance Article* as soon as it is available.

You can find more information about *Accepted Manuscripts* in the Information for Authors.

Please note that technical editing may introduce minor changes to the text and/or graphics, which may alter content. The journal's standard Terms & Conditions and the Ethical guidelines still apply. In no event shall the Royal Society of Chemistry be held responsible for any errors or omissions in this *Accepted Manuscript* or any consequences arising from the use of any information it contains.

ROYAL SOCIETY OF CHEMISTRY

www.rsc.org/loc

Lab on a Chip

RSCPublishing

ARTICLE

Functional microengineered model of the human splenon-on-a-chip

Cite this: DOI: 10.1039/x0xx00000x

Received 00th January 2012,
Accepted 00th January 2012

DOI: 10.1039/x0xx00000x

www.rsc.org/

L.G. Rigat-Brugarolas[1,2], A. Elizalde-Torrent[3], M. Bernabeu[3], M. De Niz[3], L. Martin-Jaular[3], C. Fernandez-Becerra[3], A. Homs-Corbera[1,2], J. Samitier[1,2,4+] and H.A. del Portillo[3,5+]

[1] Nanobioengineering group, Institute for Bioengineering of Catalonia (IBEC), Barcelona, Spain. [2] Centro de Investigación Biomédica en Red de Bioingeniería, Biomateriales y Nanomedicina (CIBER-BBN), Zaragoza, Spain. [3] Barcelona Centre for International Health Research (CRESIB, Hospital Clínic-Universitat de Barcelona)/ISGlobal, Barcelona, Spain. [4] Department of Electronics, Barcelona University (UB), Martí I Franques, 1, Barcelona, 08028, Spain. [5] Institució Catalana de Recerca i Estudis Avançats (ICREA), Barcelona, Spain.

+ corresponding authors:

+ Hernando A del Portillo, Ph.D. Barcelona Centre for International Health Research – CRESIB/ISGlobal, Department of Poverty-related Diseases, C/ Roselló 153 (1), Centre Esther Koplowitz Building, 08036 Barcelona, Spain. Tel +34690737229, hernandoa.delportillo@cresib.cat

+ Josep Samitier, Ph.D. Nanobioengineering group, Institute for Bioengineering of Catalonia (IBEC), Baldiri Reixac, 10-12, 08028 Barcelona, Spain. jsamitier@ibecbarcelona.eu

The spleen is a secondary lymphoid organ specialized in the filtration of senescent, damaged, or infected red blood cells. Such unique filtering capacity is largely due to blood microcirculation through filtration beds of the splenic red pulp in an open-slow microcirculation compartment where the hematocrit increases, facilitating the recognition and destruction of unhealthy red blood cells by specialized macrophages. Moreover, in sinusal spleens such as those of humans, blood in the open-slow microcirculation compartment has a uni-directional passage through interendothelial slits before reaching the venous system. This further physical constraint represents a second stringent test for erythrocytes ensuring elimination of those cells lacking deformability. With the aim of replicating the filtering function of the spleen on a chip, we have designed a novel microengineered device mimicking the hydrodynamic forces and the physical properties of the splenon, the minimal functional unit of the red pulp able to maintain filtering functions. In this biomimetic platform, we have evaluated mechanical and physiological responses of the splenon using human red blood cells and malaria-infected cells. This novel device should facilitate future functional studies of the spleen in malaria and other hematological disorders.

Lab on a Chip Accepted Manuscript

Introduction

Through a complex organizational architecture, the spleen is perfectly adapted to selectively filter and eliminate senescent red blood cells (RBCs) as well as blood-borne infectious organisms, including *Plasmodium* parasites.[1] Such complex architecture includes the splenic white pulp, red pulp, and the marginal zone, each of which is populated by specialized cells. The filtering capacity of the spleen is inherently linked to the complex vasculature of the organ, controlling events such as blood passage through the reticular meshwork of the red pulp; entry into the marginal sinuses or the marginal zone; drainage through perimarginal cavernous sinuses or capillary branches; or entry into the white pulp. The spleen's architecture is thus implicitly related to its function as the only lymphoid organ responsible for blood surveillance.

In the current microcirculation model based on washout experiments,[1] 90% of the blood-flow circulates through the spleen as closed-fast microcirculation directly bypassing the spleen's filtration capacity. The remaining 10%, however, circulates as open-slow microcirculation through the filtration beds of the cords where the hematocrit is significantly augmented, facilitating the recognition and destruction of unhealthy RBCs by macrophages.[1] Moreover, before reaching the venous system, circa 10% of the blood in the open-slow compartment of sinusal spleens, such as the human spleen, must pass through interendothelial slits (IES) of the splenic sinusoids. This passage represents a second stringent test for functionality of RBCs as less deformable unhealthy cells cannot traverse the IES.[2]

Infections by malaria parasites induce a dramatic splenic response characterized by splenomegaly. At present, our understanding of spleen pathology derives mostly from post-mortem examinations,[3] analyses of surgically removed spleens, imaging of fixed spleen sections, animal models, cellular studies and novel medical imaging techniques.[4,5] Recently, an ex vivo model of the human spleen, able to maintain clearing and processing functions was developed by Buffet *et al*.[6] Using this ex vivo system, a dual role on protection and pathology in malaria infections has been hypothesized.[7] Despite the major advance this model represents for malaria and spleen studies, its use remains limited due to the inherent difficulties for adopting it as a routine tool in the laboratory.

Advances in bioengineering and microfluidics have made it possible to achieve the necessary technology to generate patterns of complex microstructures, allowing precise control of dynamic fluid flows of small volumes. In the area of malaria research, studies of the spleen using microfluidic devices (μF-D) have been mainly utilized to study deformability of *Plasmodium*-parasitized erythrocytes (iRBCs),[8-10] cytoadhesion events, and interactions of platelets or proteins and erythrocytes with endothelial cells.[11,12] More recently, a microscale human liver platform supporting the growth of hepatic stages of human malaria parasites has been developed.[13] In the area of diagnostics, μF-D have been proposed as promising tools for malaria detection using separation principles based on the intrinsic properties of iRBCs.[14-16] Nevertheless, to our knowledge, a spleen-like microfluidic platform for the functional study of this organ has not been developed.

With the aim of studying RBCs, mature and reticulocytes (RETs), filtration in the spleen, as observed in the minimal structural functional red pulp unit, the splenon,[7] we present here a novel multilayered microengineered device of the human splenon-on-a-chip. With this device, engineered to mimic the splenic closed-fast and open-slow microcirculations, the reticular mesh where the hematocrit is augmented and the spleens's filtering function of the IES, we hope to advance our knowledge of the spleen's function in malaria and other hematological disorders.

Materials and Methods

Microfluidic model and design

A two-layer microengineered device was designed to translate a simplified but accurate version of the human spleen's red pulp human splenon (Fig. 1A). The device platform mimics the closed-fast and the open-slow microcirculations by means of two main microfluidic channels designed to provide a physiological flow division (Fig. 1B). Moreover, in the open-slow channel, blood flows through a pillar matrix resembling the reticular mesh where hematocrit is augmented. At the end of the slow-flow channel, connection to the fast-flow channel is achieved through parallel 2 μm microconstrictions resembling the IES where RBCs physically constraint before reaching the fast-flow microcirculation.

Electric circuit analogy was used to facilitate the device's design (Fig. S1), since Hagen–Poiseuille's law corresponds to Ohm's law, where the pressure drop is analogous to the voltage drop, the volumetric flow rate to the current, and the hydraulic resistance to the electric resistance.[17] The main design specifications correspond to the slow-flow channel, where, in order to mimic both the reticular mesh and the IES, we have designed, respectively, a pillar matrix constriction zone and multiple parallel microconstrictions connected to the fast–flow channel, simulating the unidirectional passage of RBCs through IES into the splenic venous system (Fig. 1B).

Lab on a Chip Accepted Manuscript

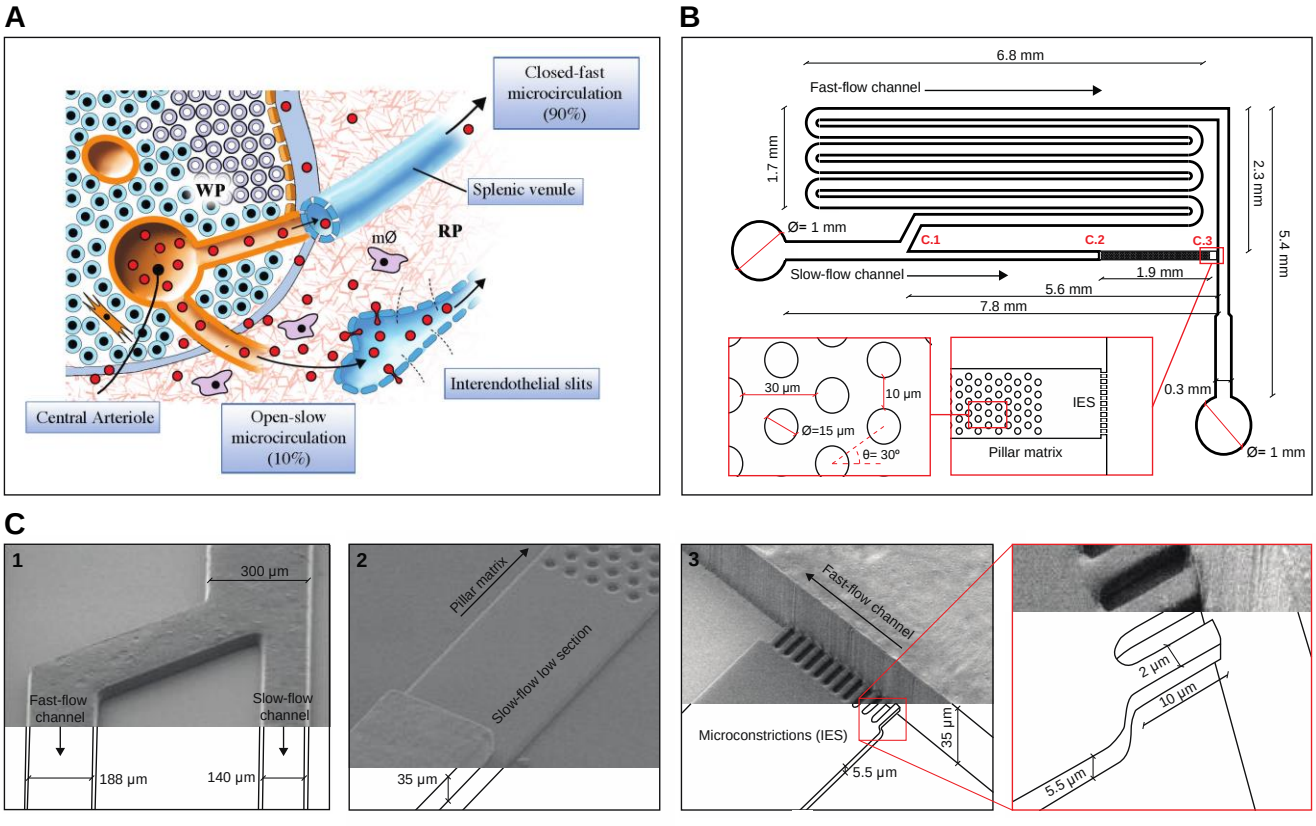

Figure 1. Microengineered model of the human splenon-on-a-chip. (A) Diagram of the human splenon showing the closed-fast and open-slow microcirculations as well as the interendothelial slits (IES). Blood in the central arteriole coming from the splenic artery may follow two different paths: (i) the closed-fast microcirculation where blood reaches directly splenic venules bypassing the spleen filtering function; (ii) the open-slow microcirculation where blood goes through the filtration beds of the cords facilitating the destruction of unhealthy RBCs by specialized macrophages (mØ). In addition, blood in the open-slow microcirculation has a unidirectional passage through IES before reaching the venous system. This further physical constraint represents a second stringent test for erythrocytes ensuring elimination of those cells lacking deformability. RP, red pulp. WP, white pulp. **(B)** Schematic representation and dimensions of the microfluidic device mimicking the human splenon, where circa 90% of the blood flows through a fast-flow channel and the remaining 10% goes through a slow-flow channel. Moreover, a pillar matrix in the slow-flow channel mimics the filtration beds of the RP before reaching the microconstrictions representing the IES. **(C)** Details and measurements of the slow-flow channel. (1) Flow division zone; (2) slow-flow low section and pillar matrix; (3) Microconstrictions representing the IES.

The flow of liquids through microfluidic channels with laminar flow usually occurs at very low Reynolds numbers (*Re*<1). To calculate R_H (hydraulic resistance) in the different branches of the device, the following equation (1) for rectangular microfluidic channel was used.

$$\Delta P = Q \bullet R_H \quad (1)$$

It establishes a relationship, for this type of devices, between Q (m^3 s^{-1}), the volumetric rate of flow of liquid between two points in a channel, and ΔP (kg m^{-1} s^{-2}), the difference in pressure between those two points. Both terms are proportional on the basis of R_H.

In a rectangular channel, the laminar flow of a single liquid phase through the channel approximately follows equation (2), where L (m) is the length of the channel, W (m) is the width of the channel, H (m) is the height of the channel, and *a* is a dimensionless parameter dependant on W/H aspect ratio, as defined in equation (3).

$$\Delta P = a\mu QL/WH^3 \quad (2)$$

$$a = 12\{1-(192H/\pi 5W)\tanh(\pi W/2H)\}^{-1} \quad (3)$$

These fluidic resistance calculations, complemented with COMSOL Multiphysics software (COMSOL AB, Sweden) simulations, were used to set the dimensions of the secondary channel reproducing the fast-flow in the biological system. The microconstrictions and the pillars matrix region were set to mimic the complex structure of the spleen in a simplified manner. Fluid flow division between fast and slow flow sections was meant to be kept near physiological values: 10-15% of flow splitting into the slow-flow channel of the model.

A first approximation to the problem was done simulating aqueous media (results shown in supplementary information,

Lab on a Chip Accepted Manuscript

Fig. S2) and values for the fast-flow channel length were estimated to be kept between 40 and 55 mm to achieve this physiological condition. However, due to the complex fluidic nature of blood, further adjustments were made experimentally.

Experimental assessment of the calculations and simulation results were initially obtained using water. Phosphate-buffered saline (PBS) medium plus fluorescent beads and blood were used later and dimensions for the fast-flow channel were fine-tuned in order to get empirically the desired flow divisions.

To obtain a spleen-like physiological behaviour inside the device the whole dimensional relations between the different elements of the device were adjusted to agree with reported measurements of human vessels in the red pulp.[1] Figure 1 shows the specific dimensions of the μF-D. The 2 μm wide and 5.5 μm high microconstrictions act as the spleen slits stretching mechanically RBCs in the planar configuration, while retaining or hinting the passage of unhealthy or infected cells. On the other hand, the pillar matrix zone consists on a 1.9 mm long section, including a total of 445 pillars with a diameter of 15 μm.

Device fabrication

The fabrication of the splenon-on-a-chip consists of a multi-step procedure designed to obtain two different heights using two different photoresists by means of photo-lithographic and soft-lithographic techniques customized for fabricating a multilayer platform. All works were carried out in the clean room facility of the Institute for BioEngineering of Catalonia (IBEC).

All solvents and chemical were obtained from Sigma Aldrich unless otherwise specified. SU-8 photoresist and developer were from MicroChem (Newton, MA). Ordyl photoresist and developer were from Elga (Italy).

The master is fabricated over glass slides (Fig. 2A-1). A thoroughly cleaning protocol based on chemical baths and surface activation process is used for the slides. The process starts with three consecutive solvent baths of acetone, isopropanol and ethanol. Then, after dehydration, the glass surface is subjected to 10 W of O_2 plasma power for 10 minutes to improve photoresist adhesion. Following the cleaning protocol, the first step to shape the master consists of patterning Ordyl SY 330 alignment marks for a correct structuring of the bilayer device (Fig. 2A-[2-5]). The slide is then gyrated and following processes are performed on the plain side (Fig. 2A-6). This is done to avoid mask contact problems and resolution loses arising from Ordyl features height during the following microfabrication steps. Then, the cleaning procedure is repeated and a layer of SU-8 2000.5 is spun (500 nm). This layer will act as an interface between glass and further photoresist layers (Fig. 2A-[7,8]).

Later, in order to fabricate the first layer of the device (slow-flow channel), a 5.5 μm-high SU-8 10 negative photoresist is spun over the glass slide applying a three-step spinning protocol to obtain the desired SU-8 thickness (Fig. 2A-9). The slide is then soft-baked on a hot plate before being exposed with a chrome-on-glass photomask to UV Light (4 s, 24 mW cm^2, 345 nm) in a mask aligner (MJB4 aligner, SÜSS Microtec, Germany). After that, the slide is baked in the sequence of 65ºC for 1 minute and 95ºC for 3 minutes, left to cool for up to 1 hour, and finally developed using the SU-8 developer for 30 s (Fig. 2A-[10-12]).

For the second device layer (fast-flow channel), Ordyl SY330 negative photoresist is laminated on top of the last SU-8 layer using a hot/cold laminator in order to have a smooth attached 35 μm-high film surface (Fig. 2A-13). Then, the slide is exposed through an acetate photomask to UV light (5 s, 24 mW cm^2, 345 nm) in the mask aligner, and subsequently placed on a hot plate at 65ºC for 3 minutes (Fig. 2A-[14,15]). The master three-dimensional mould fabrication is finished by developing the Ordyl film using the Ordyl developer for 3 minutes (Fig. 2A-16).

To replicate the master's microchannels, a PDMS pre-polymer mixture (curing agent-to-PDMS ratio of 1:10, Sylgard®184, Dow Corning) is placed in a desiccator and vacuum applied in order to remove bubbles. Then, the mixture is poured on top of the SU-8/Ordyl master to fabricate a PDMS mould, heated up at 65ºC for 3 hours and afterwards kept at room temperature for 24 hours. The casted PDMS is peeled off carefully and inlet and outlet holes are made using a Harris Uni-Core 1 mm puncher. After cleaning, both the glass and the PDMS structures are chemically modified in O_2 plasma and immediately pressed together to form a permanent bond (Fig. 2B).

Uninfected red blood cells

Mature human red blood cells were obtained from donors at the Blood and Tissue Bank (Barcelona), after written consent and in accordance with the ethics Committee protocols of the Blood and Tissue Bank. Upon receipt, RBCs were washed twice with incomplete RPMI and re-suspended at a 50% hematocrit in the same medium. RBCs were immediately used or maintained at 4ºC for seven weeks before deformability measurements. For microfluidics experiments, aliquots of 500 μl were injected into the microfluidic system.

Lab on a Chip Accepted Manuscript

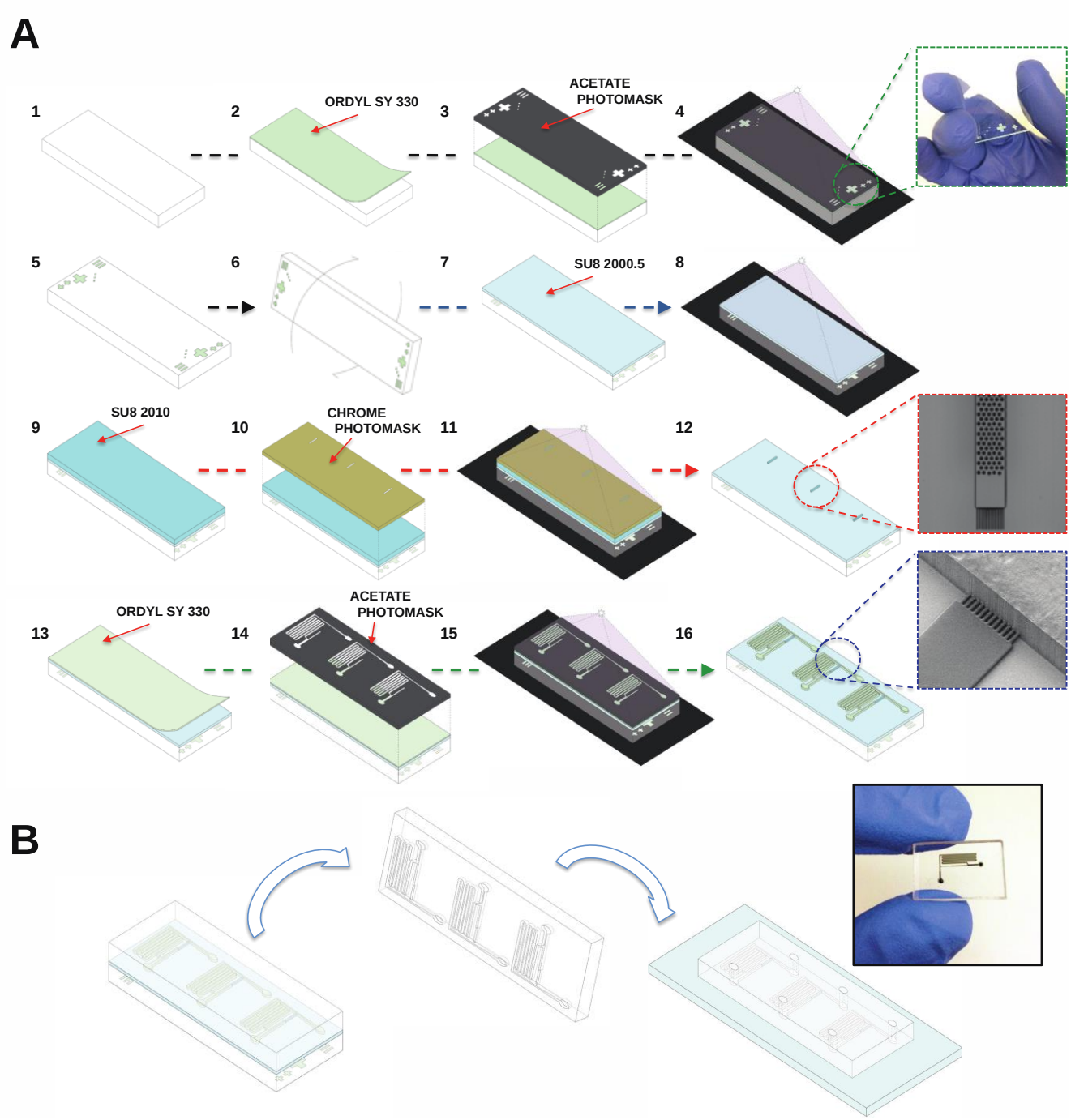

Figure 2. Schematic of the fabrication. The fabrication of the splenon-on-a-chip consists of a multi-step procedure. **(A)** Shows the SU-8/Ordyl master fabrication process. **(B)** Master replication process using PDMS bonded to glass to finally obtain the splenon-on-a-chip biomimetic platform.

Infected red blood cells

The reticulocyte-prone *Plasmodium yoelii*-GFP transgenic line was generated as described elsewhere.[18] For mice infections, female BALB/c of 6-8 weeks of age (Charles River Laboratories) were infected by intraperitoneal injection of $5x10^5$ RBCs obtained from the tail blood of donor mice at 5-10% parasitemia. Parasitemia was then monitored through Giemsa staining of blood smears until reaching the desired levels (80 to 85% of infected RETs). Cells were finally counted in different optical fields adding up to at least 1500.

Blood from mice was collected in EDTA by intracardiac puncture of infected mice on day 11 post-infection and then passed through a CF11 cellulose filter and washed with PBS in order to remove leukocytes. Blood smears were done to check the efficiency of the CF11 column and to verify the percentage

Lab on a Chip Accepted Manuscript

of infected RETs. RBCs were re-suspended in RPMI at a 50% hematocrit and injected into the microfluidic system. All studies involving mice were performed at the animal facilities of Hospital Clinic in Barcelona in accordance with guidelines and protocols approved by the Ethics Committee for Animal Experimentation of the University of Barcelona (CEEA-UB).

Physiological flow rate

The physiological flow rate imposed in our device was obtained after analyses of intravital images of the spleen of Balb/c mice injected with FITC-labelled RBCs in order to quantify velocity of RBCs in the small vessels just before reaching the open circulation in the red pulp.[19] Spleens were exposed and visualized under a high-speed multiphoton confocal microscope fitted with an inverted 63x glycerol objective. Vessels were set horizontally by optical field rotation and images were acquired using xy and xt line-scanning modes in the central lumen of the vessel. Bidirectional scanning with a line average of 32 was used at a speed of 8 kHz and an image of 512 pixels × 512 lines was obtained as described before.[19] In these images, the slope of fluorescent streaks resulting from moving cells was used to quantify velocities. Intravital microscopy of 10 spleen vessels with 7 ± 0.6 μm of diameter was performed and a velocity of 740 μm/s was estimated.

Experimental system operation

The experimental setup consists of a 1 ml syringe (BD Plastipak) connected through a needle (BD 23G 1" Nr. 16, 0.6 x 25 mm) with PTFE tubing (ChipShop, Jena, Germany) to the μF-D. The syringe is actuated with a KDS 200 series pump (catalogue no. 78-9202). Tubes were inserted into the access holes, which were slightly smaller than the outer diameter of the tubing to form a pressure seal between the tubing and the hole (Fig. S3). A constant flow of 5 μl/min was established on the μF-D. Experiments with buffers and beads were carried out at room temperature whereas experiments with RBCs and iRBCs were carried out at physiological temperature of 37ºC.

Concerns regarding the formation of bubbles inside the device were faced during the experimentation. Consequently, precautions were taken before each experiment while handling blood samples with the syringe, eliminating all possible bubbles both in the syringe and the tubing connected to the μF-D. With this methodology, bubbles apparition inside the device was prevented.

Image capture and analysis

Optical measurements for microfluidic analyses were performed using an inverted optical microscope (Olympus IX71) with an integrated CCD Hamamatsu camera. Optical measurements of iRBCs were obtained using a laser scanning confocal microscope (TCS-SP5; Leica Microsystems) at a magnification of 25.0x (water objective). Several movies of 10s were recorded of blood microcirculation in the device. Bright field and fluorescence were acquired in two different channels (excitation/emission wavelength 488/505-580 for GFP). Videos were analyzed using ImageJ software (version 1.41n, Wayne Rasband, NIH).

Measurement of cell deformability

Optical microscopy and intravital imaging were used to obtain deformability measurements of individual cells in the slow compartment as well as while passing through the slits using ImageJ processing and analysis software. Three measures of each cell were obtained. Cell deformability was calculated measuring the elongation of blood cells (using high-speed/resolution microscopic videos) inside the slits in the X-axis, the axis parallel to the flow direction (since the deformation in the Y-axis is always going to be of 2 μm). This technique resembles what some authors refer to as "hydropipetting".[20] The deformation measurement ($D_{M\%}$) is therefore defined as the percentage of difference between the length in microns of a single cell in the slit (L_S) and the length in the pillar matrix zone (L_{RM}), as is shown in equation 4.

$$D_{M\%} = [(L_S - L_{RM})/ L_{RM}] \bullet 100 \quad (4)$$

Statistical analysis

The median (M_{ed}) and the quartiles of the length and the deformation of the cells were analyzed using Microsoft Excel and IBM SPSS statistics program. Because statistical analysis entails comparing two different cell populations, non-parametric Mann–Whitney *U* statistical test was used.

RESULTS AND DISCUSSIONS

Flow dynamics measured using microbeads

The hydrodynamic behaviour of the device was tested and verified with microbeads (Polysciences, Inc., Warrington, PA) of different diameters (ranging from ∅=1.8 μm to 8 μm) diluted in PBS. These initial assays focused on the critical sections of the μF-D to confirm that flow motion and division in the device was similar to that of the actual spleen on a proportional scale (Fig. S4-A). Also it was pivotal to examine the demeanor of the pillar matrix section to confirm that it acted as a particle retention mechanism, not as a deterministic lateral displacement step, reducing the particle speed while increasing the cell density (Fig. S4-B). Once these trials were completed, adaptations on the device structure were done in order to work with a non-Newtonian physiological fluid like blood.

Lab on a Chip Accepted Manuscript

Physiological flow division

The blood circulation pattern within the human spleen has been recently investigated *in vivo* by means of contrast-enhanced ultrasonography.[21] Noticeably, the data showed and confirmed a dual microcirculatory organization with approximately 10% of the blood input flowing through a slow compartment whereas the remaining 90% flow goes through a fast compartment. Hydrodynamic studies were thus performed to accurately translate the organ's flow behaviour inside the μF-D. Of significance, microfluidic analyses confirmed that the design of the device mimicked the two-compartment blood circulation of the human spleen, with the channel representing the slow-flow accounting for approximately 10% of the flow (Fig. 3 and supplementary movie 1).

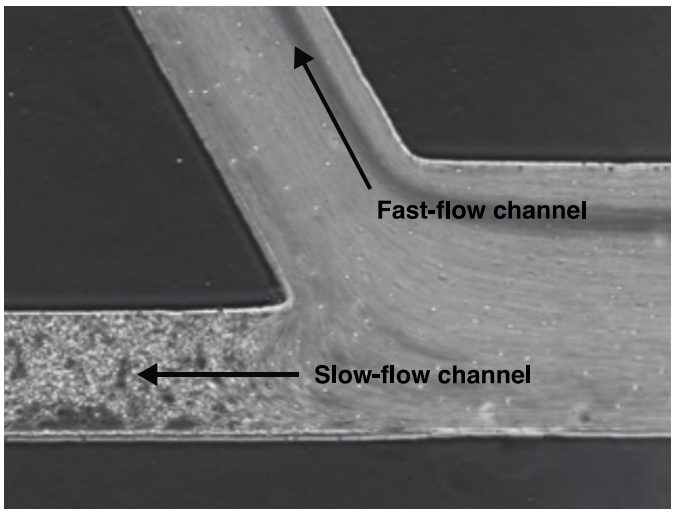

Figure 3. Blood flow division inside the microfluidic device. Images showing that the 90% of the blood flow goes through the fast-flow channel whereas the remaining 10% goes through the slow-flow channel. Images were taken using an inverted optical microscope (Olympus IX71) with an integrated CCD Hamamatsu camera.

Physiological flow rate

Different flow rates (*q*) using human whole blood were tested and studied using diverse μF-D structures, and a value of *q*=5 μl/min was seen to translate similar velocities in the zone before the constriction slits of the slow-flow channel as the ones obtained through *in vivo* imaging of the spleen of mice. Therefore in our system we have achieved an architecture such that the velocity (*v*) in that specific section is similar to physiological velocity, in the *v*=120–760 μm/s range, depending on the channel's position of the RBCs. Furthermore, the designed structure of the device maintains a physiological Reynolds number in the channels (*Re*=0.15) and ensures negligible RBCs lysis at that flow rate inside the chip.

Hematocrit in the slow-flow channel

Increase in hematocrit value (HCT) is observed in the reticular mesh of the spleen.[1] To mimic this reticular mesh, we have included a pillar matrix zone in the slow-flow compartment to further impede the flow increasing the cell's density and therefore the HCT in that compartment. This entails that the RBCs density (δ) increases with the passage of time until the scenario arrives to the equilibrium (Fig. 4). This fact is manifestly described in the difference of number of cells between the pre-low height section and the pillar zone, where the density clearly increases, from δ≈0.007 RBCs/μm^2 to 0.02 RBCs/μm^2, respectively.

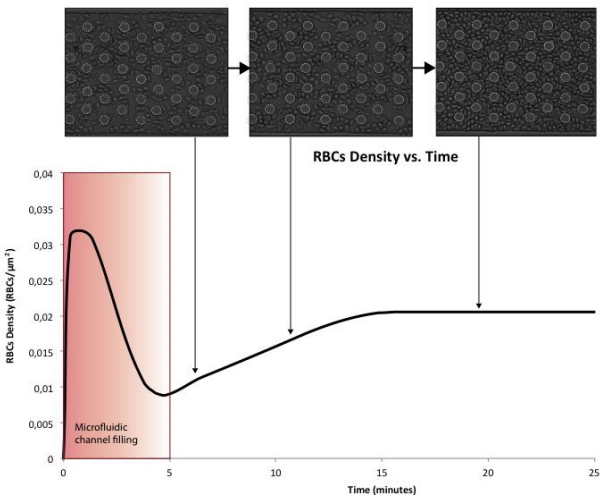

Figure 4. Red blood cell density versus time in the pillar matrix section of the slow-flow channel. Upper panel. Time-series images of the pillar matrix in the slow-flow channel showing the increase of RBCs density. **Lower panel.** After the initial minutes required for the microfluidic channel filling, the graphic shows the increase of RBCs per μm^2 along the time.

Deformability of studied cells

Following the validation of the physiological flow rate, deformability tests of fresh and aged human RBCs were performed (Fig. 5A). Using the Mann-Whitney *U* test (with n=130 for each population), we observed a statistically significant difference between the deformation percentage of old (Med=26.9%) and fresh RBCs (Med=38.3%) passing through the 2 μm microconstrictions mimicking the IES (*p*=0.001, Fig. 5B). This is consistent with the expectation that old/senescent RBCs are significantly less deformable than younger RBCs.[2]

Lab on a Chip Accepted Manuscript

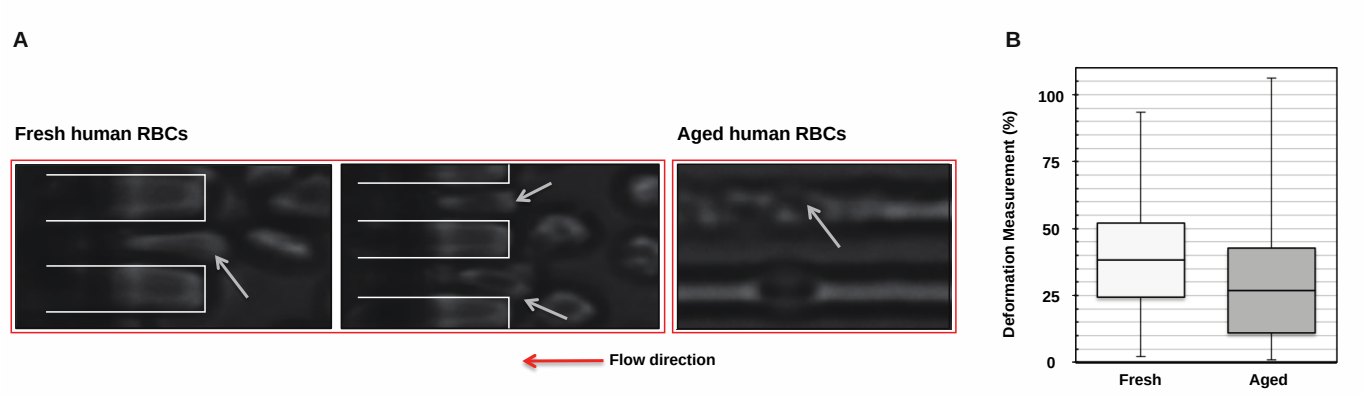

Figure 5. Deformability of fresh and aged RBCs inside the slow-flow channel of the μF-D. **(A)** Transit of fresh and aged RBCs through the microconstrictions in the slow-flow channel mimicking the IES. The red arrow indicates blood flow direction. White arrows point to RBCs inside the microconstrictions. White squares represent physical borders of the microconstrictions. **(B)** Graph showing the median and the quartiles of the deformation percentage of fresh and aged RBCs populations. Data was analyzed using Mann-Whitney *U* test (p=0.001).

Having made this observation with human RBCs, deformability measurements were then performed with blood cells from BALB/c mice infected with *P. yoelii* 17X constitutively expressing GFP to facilitate image acquisition (Fig. 6A and supplementary movies S2 and S3). We decided to use this transgenic line since it has a tropism for RETs known to be highly deformable upon infection with RET-prone malarial parasites.[23] *P. yoelii*-infected RETs were easily detected in phase contrast images in the slow-flow channel before, during, and after passage through the 2 μm microconstrictions.

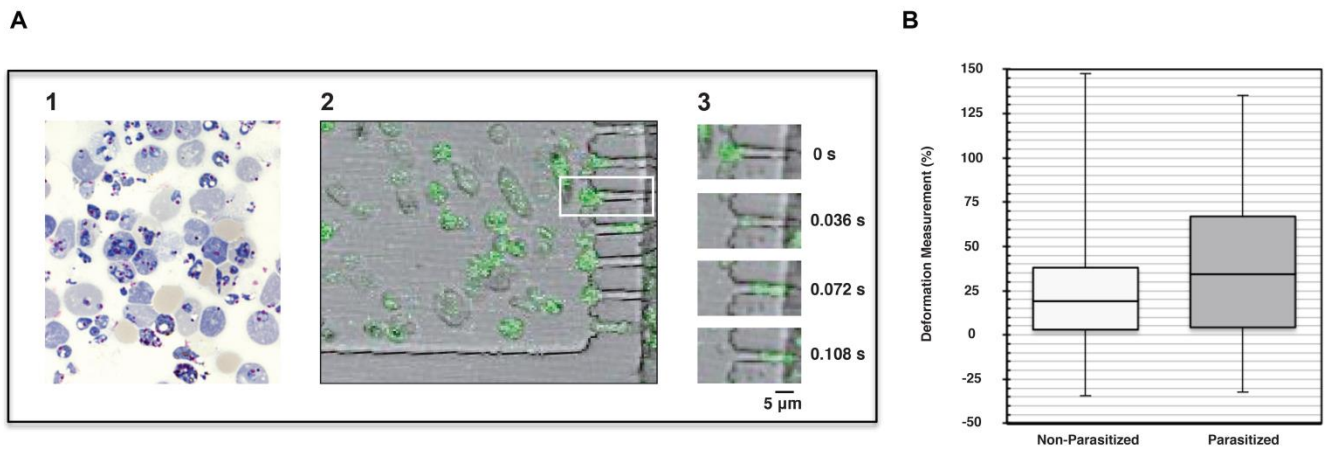

Figure 6. Deformability of parasitized and non-parasitized RBCs inside the slow-flow channel of the μF-D. (A) Transit of blood from *P. yoelii* RET-prone non-lethal strain (17X-GFP) infected mice through the microconstrictions in the slow-flow channel. (1) BCB-Giemsa blood smear from a BALB/c mouse experimentally infected with 17X-GFP strain. An approximate 80% of infected red blood cells (all RETs) are shown in this field. Image was taken with Nikon Eclipse 50i 100x/1.30 oil with a DS-U2 controller. (2) CCD-image showing *P. yoelii*-GFP-infected RETs in the slow-flow channel and passing through the microconstrictions. (3) Time lapse-series showing the passage of one infected RET (green) going through a microconstriction. **(B)** Graph showing the median and the quartiles of the deformation percentage of parasitized and non-parasitized RBCs. Data was analyzed using Mann-Whitney U test (p=0.006).

Measurements of iRBCs and RBCs inside and outside the slits revealed a highly significant difference in deformation percentage of infected reticulocytes (Med=34.3% and 19.1% each) using Mann-Whitney *U* test (n=130, p=0.006) (Fig. 6B). Moreover, it was observed that the length of iRBCs and RBCs, both in the slits (Med=9.06 μm and 7.62 μm) and in the pillar matrix zone (Med=6.74 μm and 6.4 μm), showed statistically significant differences using de Mann-Whitney *U* test, with a value of p<0.0001 and p=0.002 respectively, thus indicating a larger dimension of iRBCs on average.

Lab on a Chip Accepted Manuscript

Discussions

The minimal functional unit of the red pulp able to maintain filtering functions has been termed the splenon.[7] In this work, we present a novel multilayered microfluidic device of a human splenon-on-a-chip for advancing studies of the role of the spleen in malaria and other hematological disorders.

The rheological properties of RBCs during hematological disorders, including malaria, have been studied using various techniques.[24,25] Of particular relevance are the studies on RBCs deformability upon malarial infections, as several attempts have been made to associate deformability changes with pathology. Cell deformability is determined by three principal components: viscoelastic properties of the cytoplasmic membrane, geometry of the cell and intracellular viscosity.[26] All these components have been taken into consideration to study RBCs deformability in malaria. Pioneering studies using filtration methods suggested that iRBCs lack structural deformability and could thus contribute to blockage of capillaries.[27] Ektacytometry measurements determined under fluid, generate physical modifications of the ratio of a cell´s length to width (deformability index) and have been proposed as of prognostic value on severe malaria.[28] The deformability of iRBCs has also been determined after micropipette aspiration.[26] In addition, optical tweezers have measured deformability of iRBCs upon physical stretching of individual cells and shown that individual proteins can reduce the deformability of infected cells at particular *Plasmodium* intraerythrocytic developmental stages.[29-31]

Microfluidic devices brought into these studies the possibility of performing individual cell deformability measurements in real-time. Thus, by constructing channels of different sizes and recording the passage of iRBCs, results demonstrated that ring-stages pass freely through all size-channels whereas trophozite-infected and schizont-infected RBCs failed to traverse 2-to-4 μm channels.[9] More sophisticated devices and imaging quantification approaches have recently demonstrated that the geometry of the cell plays a fundamental role in its passage through the spleen.[11,32,33]

Unlike any previous device, the human splenon-on-a-chip incorporates for the first time two compartments with differences in flow velocities and two physical barriers representing the reticular mesh and the IES where cells first slow down increasing the HCT and then traverse the IES in a unidirectional manner. Thus, cells in the suspension are likely deformed by a combination of several hydrodynamic forces. Mainly because of these reasons, we calculated cell deformability measuring the elongation of blood cells, a technique that resembles what some authors refer to as "hydropipetting".[20] We believe this procedure to be the most accurate and precise to obtain the measurements required by our system, where multiple cells pass through the same slit under different hydrodynamic forces in a very short period of time.

To demonstrate the validity of such methodology, we showed that old RBCs are less deformable than freshly drawn RBCs, which is consistent with previous studies.[9] Moreover, to better capture, model and quantify the deformability and passage of iRBCs through the IES using this statistical method, we used peripheral blood of BALB/c mice experimentally infected with the *P. yoelii* 17X-GFP strain. This strain has a tropism for reticulocytes and constitutively expresses GFP throughout the intraerythrocytic developmental cycle facilitating image acquisition and quantification. Results demonstrated that infected reticulocytes are significantly more deformable than non-infected reticulocytes. This is in agreement with the higher deformability of infected reticulocytes reported for *P. vivax*, a human malarial parasite with reticulocyte tropism.[23]

A potential limitation of the device is the current slit size (2 μm width, 10 μm length and 5.5 μm height), as it seems that slits in the human spleen might be smaller.[34] Noticeably, *in vivo* imaging of the dynamic passage of malarial parasites in the rat sinusal spleen elegantly demonstrated that IES remain closed for long periods of time, that only around 15% are open in any one particular 5 min, and that the size of the IES vary from wide open, allowing the passage of RBCs without any physical constraint, to scarcely open, where RBCs need to squeeze to reach the venous flow.[34] Moreover, these studies also showed that there is la large variation in transit times of RBCs through the IES (0.02 s to 60.5 s); yet, 87% of the RBCs had a transit time less than the mean, 1.71 s. Observations of the dynamic passage of iRBCs in our device demonstrated similar variability in the transit times as well as the unidirectionality of flow (supplementary movies S2 and S3) therefore agreeing with the passage of RBCs through IES *in vivo* in the sinusal spleen.[35]

Experiments during more than 60 min have been performed and the μF-D did not present any leakage or rupture of its structure. Since the dimensions of the device's channel and the flow rate imposed in the system corresponds to physiological values, the cells flowing in the system stay variable through its transit in the different parts of the platform. Trials increasing the entrance flow rate (over physiological conditions) showed a breakage in cell's membrane in the slow-flow channel.

In a recent study, micro-sphere beads with two different size distributions (5-to-15 μm and 15-to-25 μm diameters) were mixed to create an *in vitro* matrix mimicking the human spleen IES.[34] After mixing the beads, an approximate one micron pore size was obtained resembling the size of the IES, as determined by SEM of 11 spleens. Thus, this device forces the passage of individual RBCs and iRBCs through several "slits". In spite this major difference with the *in vivo* situation, results on trapping by this device paralleled trapping on an *ex vivo* model of the human spleen. Future studies of field isolates on rheological properties of RBCs during malaria infections comparing the column device and the human splenon-on-a-chip are envisioned. In addition, in order to better mimic real physiological conditions in blood vessels, reflecting the fluctuating flow rate of the blood stream in the human body, the use of pulsatile pumps are foreseen.

A step forward in this field concerns organ-on-a-chip devices. The integration of such biomimetic platforms

Lab on a Chip Accepted Manuscript

mimicking physiological conditions has the potential to enable user-friendly and low-cost experimental lab-on-a-chip devices.[36] In this sense, great efforts have been directed in recent years towards developing organ models on a chip that permit the investigation of both biological and physiological features.[37]

Many successful devices have been already developed in the area of organ-on-a-chip technology structures.[36-38] The construction of a functional human splenon-on-a-chip represents a first step in the long-term goal of construction a functional 3D model of the human spleen-on-a-chip.

Conclusions

We have developed a newfangled microfluidic device of a human splenon-on-a-chip that mimics the hydrodynamic behaviour of the organ and its filtering functions. Unlike any other previous μF-D, the human splenon-on-a-chip incorporates for the first time two compartments with difference in flow velocities (together with the correct physiological flow division) and two physical barriers representing the reticular mesh and the IES where cells first slow down increasing the HCT and then traverse the IES in a unidirectional matter. This biomimetic-chip based platform should help in have a deeper understanding of the molecular basis of spleen pathophysiology in human malaria and other hematologic disorders. The system might also provide a flexible platform to screen for potential drugs in hematologic disorders.

To validate the use of this platform, several experiments were carried out with different types of blood cells. As a proof of concept, we showed that old RBCs (as expected) showed less deformability than freshly drawn RBCs when traversing the microconstrictions. Posterior analysis allowed studying the passage and deformability of iRBCs through the IES using peripheral blood of BALB/c mice experimentally infected with the *P. yoelii* 17X-GFP strain. Results demonstrated that infected reticulocytes are significantly more deformable than non-infected reticulocytes, in agreement with the higher deformability of infected–reticulocytes of *P. vivax*, a human malarial parasite with reticulocyte tropism. In addition, the length of iRBCS and RBCs showed statistically significant differences in the pillar matrix zone. This result suggests that the device, on the one hand, is able of reproducing physiological conditions, and on the other, the capability of distinguish different types of RBCs by means of deformation/mechanical properties.

Acknowledgements

Funded by the EXPLORA Programme of the Ministry of Economy and Competitiveness of the Government of Spain (SAF2012-35133). Part of this work was also supported by the technology transfer program of the Fundación Botín and by the European Community's Seventh Framework Programme (grant agreement N° 242095). We thank David Izquierdo, Miriam Funes, Juan Manuel Álvarez, Miriam Ramirez and Maria Calvo for their technical help in this project.

Electronic Supplementary information

Electronic Supplementary Information (ESI) available: Fig. S1, Fig. S2, Fig. S3 and Fig. S4. Supplementary movies S1, S2, and S3. See DOI: 10.1039/b000000x/

References

1. A. J. Bowdler, The Complete Spleen, Humana Press, 2nd edition. 2002.
2. N. Mohandas and P. G. Gallagher, Blood, 2008, 112, 3939-3948.
3. B. S. Wilkins, British journal of haematology, 2002, 117, 265-274.
4. C. R. Engwerda, L. Beattie and F. H. Amante, Trends in parasitology, 2005, 21, 75-80.
5. H. A. Del Portillo, M. Ferrer, T. Brugat, L. Martin-Jaular, J. Langhorne and M. V. Lacerda, Cellular microbiology, 2012, 14, 343-355.
6. P. A. Buffet, G. Milon, V. Brousse, J. M. Correas, B. Dousset, A. Couvelard, R. Kianmanesh, O. Farges, A. Sauvanet, F. Paye, M. N. Ungeheuer, C. Ottone, H. Khun, L. Fiette, G. Guigon, M. Huerre, O. Mercereau-Puijalon and P. H. David, Blood, 2006, 107, 3745-3752.
7. P. A. Buffet, I. Safeukui, G. Deplaine, V. Brousse, V. Prendki, M. Thellier, G. D. Turner and O. Mercereau-Puijalon, Blood, 2011, 117, 381-392.
8. Q. Guo, S. J. Reiling, P. Rohrbach and H. Ma, Lab on a chip, 2012, 12, 1143-1150.
9. J. P. Shelby, J. White, K. Ganesan, P. K. Rathod and D. T. Chiu, Proceedings of the National Academy of Sciences of the United States of America, 2003, 100, 14618-14622.
10. S. Handayani, D. T. Chiu, E. Tjitra, J. S. Kuo, D. Lampah, E. Kenangalem, L. Renia, G. Snounou, R. N. Price, N. M. Anstey and B. Russell, The Journal of infectious diseases, 2009, 199, 445-450.
11. T. Herricks, K. B. Seydel, G. Turner, M. Molyneux, R. Heyderman, T. Taylor and P. K. Rathod, Lab on a chip, 2011, 11, 2994-3000.
12. M. Antia, T. Herricks and P. K. Rathod, PLoS pathogens, 2007, 3, e99.
13. S. March, S. Ng, S. Velmurugan, A. Galstian, J. Shan, D. J. Logan, A. E. Carpenter, D. Thomas, B. K. Sim, M. M. Mota, S. L. Hoffman and S. N. Bhatia, Cell Host Microbe, 2013, 14, 104-115.
14. P. Gascoyne, C. Mahidol, M. Ruchirawat, J. Satayavivad, P. Watcharasit and F. Becker, Lab on a chip, 2002, 2, 70-75.
15. P. A. Zimmerman, J. M. Thomson, H. Fujioka, W. E. Collins and M. Zborowski, The American journal of tropical medicine and hygiene, 2006, 74, 568-572.
16. H. Bow, I. V. Pivkin, M. Diez-Silva, S. J. Goldfless, M. Dao, J. C. Niles, S. Suresh and J. Han, Lab on a chip, 2011, 11, 1065-1073.
17. K. W. Oh, K. Lee, B. Ahn and E. P. Furlani, Lab on a chip, 2012, 12, 515-545.
18. L. Martin-Jaular, M. Ferrer, M. Calvo, A. Rosanas-Urgell, S. Kalko, S. Graewe, G. Soria, N. Cortadellas, J. Ordi, A. Planas, J. Burns, V. Heussler and H. A. del Portillo, Cell Microbiol, 2011, 13, 109-122.
19. M. Ferrer, L. Martin-Jaular, M. Calvo and H. A. Del Portillo, Journal of visualized experiments: JoVE, 2012, DOI: 10.3791/36093609 [pii].
20. J. S. Dudani, D. R. Gossett, H. T. Tse and D. Di Carlo, Lab Chip, 2013, 13, 3728-3734.
21. I. Safeukui, J. M. Correas, V. Brousse, D. Hirt, G. Deplaine, S. Mule, M. Lesurtel, N. Goasguen, A. Sauvanet, A. Couvelard, S. Kerneis, H. Khun, I. Vigan-Womas, C. Ottone, T. J. Molina, J. M. Treluyer, O. Mercereau-Puijalon, G. Milon, P. H. David and P. A. Buffet, Blood, 2008, 112, 2520-2528.
22. B. M. Cooke, N. Mohandas and R. L. Coppel, Advances in parasitology, 2001, 50, 1-86.

Lab on a Chip Accepted Manuscript

23. R. Suwanarusk, B. M. Cooke, A. M. Dondorp, K. Silamut, J. Sattabongkot, N. J. White and R. Udomsangpetch, The Journal of infectious diseases, 2004, 189, 190-194.
24. M. Antia, T. Herricks and P. K. Rathod, Cellular microbiology, 2008, 10, 1968-1974.
25. J. Stuart and G. B. Nash, Blood reviews, 1990, 4, 141-147.
26. G. B. Nash, E. O'Brien, E. C. Gordon-Smith and J. A. Dormandy, Blood, 1989, 74, 855-861.
27. L. H. Miller, S. Usami and S. Chien, The Journal of clinical investigation, 1971, 50, 1451-1455.
28. A. M. Dondorp, P. A. Kager, J. Vreeken and N. J. White, Parasitol Today, 2000, 16, 228-232.
29. S. Suresh, J. Spatz, J. P. Mills, A. Micoulet, M. Dao, C. T. Lim, M. Beil and T. Seufferlein, Acta biomaterialia, 2005, 1, 15-30.
30. J. Sleep, D. Wilson, R. Simmons and W. Gratzer, Biophysical journal, 1999, 77, 3085-3095.
31. J. P. Mills, M. Diez-Silva, D. J. Quinn, M. Dao, M. J. Lang, K. S. Tan, C. T. Lim, G. Milon, P. H. David, O. Mercereau-Puijalon, S. Bonnefoy and S. Suresh, Proceedings of the National Academy of Sciences of the United States of America, 2007, 104, 9213-9217.
32. T. Herricks, M. Antia and P. K. Rathod, Cellular microbiology, 2009, 11, 1340-1353.
33. T. Herricks, K. B. Seydel, M. Molyneux, T. Taylor and P. K. Rathod, Cellular microbiology, 2012, 14, 1880-1891.
34. C. Lavazec, G. Deplaine, I. Safeukui, S. Perrot, G. Milon, O. Mercereau-Puijalon, P. H. David and P. Buffet, Methods Mol Biol, 2013, 923, 291-297.
35. I. C. MacDonald, D. M. Ragan, E. E. Schmidt and A. C. Groom, Microvasc Res, 1987, 33, 118-134.
36. D. Huh, B. D. Matthews, A. Mammoto, M. Montoya-Zavala, H. Y. Hsin and D. E. Ingber, Science, 2010, 328, 1662-1668.
37. D. Huh, H. J. Kim, J. P. Fraser, D. E. Shea, M. Khan, A. Bahinski, G. A. Hamilton and D. E. Ingber, Nature protocols, 2013, 8, 2135-2157.
38. S. A. Lee, Y. No da, E. Kang, J. Ju, D. S. Kim and S. H. Lee, Lab on a chip, 2013, 13, 3529-3537.

Lab on a Chip Accepted Manuscript